EARTHQUAKE SPECTRA

The Professional Journal of the Earthquake Engineering Research Institute

PREPRINT

This preprint is a PDF of a manuscript that has been accepted for publication in *Earthquake Spectra*. It is the final version that was uploaded and approved by the author(s). While the paper has been through the usual rigorous peer review process for the Journal, it has not been copyedited, nor have the figures and tables been modified for final publication. Please also note that the paper may refer to online Appendices that are not yet available.

We have posted this preliminary version of the manuscript online in the interest of making the scientific findings available for distribution and citation as quickly as possible following acceptance. However, readers should be aware that the final, published version will look different from this version and may also have some differences in content.

The DOI for this manuscript and the correct format for citing the paper are given at the top of the online (html) abstract.

Once the final, published version of this paper is posted online, it will replace the preliminary version at the specified DOI.

Out-of-Plane Dynamic Stability of Unreinforced Masonry Walls in One-Way Bending: Shake Table Testing

Osmar Penner[1] and Kenneth J. Elwood[2], M.EERI

Given sufficient anchorage to the diaphragms, an unreinforced masonry (URM) wall subjected to out-of-plane inertial forces will likely develop a horizontal crack at an intermediate height about which the wall will rock as semi-rigid bodies. The effect of wall slenderness on out-of-plane stability has been demonstrated in past studies, but treatment of the effects of diaphragm flexibility and ground motion variability has been limited. This paper presents an experimental study examining the out-of-plane stability under seismic loading of URM walls connected to flexible diaphragms. Five full-scale unreinforced solid clay brick wall specimens spanning one storey were subjected to earthquake ground motions using a shake table. The top and bottom of the walls were independently connected to the shake table through coil springs, simulating the flexibility of diaphragms. Variables examined experimentally included diaphragm stiffness and wall height. Both the amount of rocking observed as well as the ground motion scale causing collapse varied significantly with changes in the diaphragm properties. The test results provided data used for validation of a rigid-body rocking model, enabling an extensive parametric study on wall stability and the development of new assessment guidelines in a companion paper.

INTRODUCTION

A significant stock of unreinforced masonry (URM) buildings is present throughout the world, including seismically active regions in Canada, the United States, and New Zealand. URM buildings from these regions and representative of those considered in this study were constructed in the late 1800s to early 1900s, and typically have a simple, usually rectangular footprint with minimal vertical irregularities. Exterior walls are constructed of clay brick and consist of multiple wythes (vertical sections of masonry one brick thick). Bricks could

[1]BC Hydro, 6911 Southpoint Drive, Burnaby, B.C. Canada V3N 4X8
[2]Dept. of Civil and Environmental Engineering, University of Auckland, 3 Grafton Road, Auckland, New Zealand

be laid in a number of possible bond patterns, but the wythes are tied together intermittently by headers (bricks laid perpendicular to the wall, so that one brick spans two wythes).

This study focuses on URM bearing wall buildings with flexible timber diaphragms; for the typology considered, diaphragms are typically timber joists (or trusses) sheathed with narrow ($\sim 150\,$mm) boards nailed to the joists. These flexible diagrams impact the seismic performance of URM buildings in numerous ways, including: modifying the fundamental period; varying displacements along the length of out of plane walls; and, interacting with walls during out of plane rocking response. The latter is the focus of this study.

EARTHQUAKE PERFORMANCE OF URM BUILDINGS

URM buildings have performed consistently poorly in past earthquakes. Typical damage includes chimney, parapet, and gable failures, in-plane wall failures due to sliding or diagonal shear, toe crushing, or rocking, and out-of-plane wall failures. Past earthquakes have demonstrated out-of-plane wall failure to be the most common failure mode as well as the mode presenting the greatest life safety hazard [Bruneau and Lamontagne, 1994, Dizhur et al., 2011]. Extensive in-plane damage has also been observed, particularly shear cracking in piers and spandrels. While such damage affects the lateral load-carrying capacity of a building, gravity loads can remain supported even under large lateral displacements [Russell et al., 2013]. In-plane damage by itself thus often does not lead to collapse without excessive deformations or accompanying out-of-plane failure.

Vintage URM buildings often have limited or no lateral connections between load-bearing walls and floor and roof diaphragms. This leads to walls essentially falling off the building by tipping over when subjected to ground shaking, in what is termed a ‘cantilever’ out-of-plane failure. If walls are adequately anchored to diaphragms at each level, this failure mode is prevented, and out-of-plane failures occur by bending of the wall between support points. Where limited vertical supports are present between floors, such as in long walls or in piers between windows, walls can fail in one-way vertical bending — spanning between adjacent diaphragms. Where vertical supports are significant (e.g., cross walls, corners), walls can fail in two-way bending. All three failure modes (cantilever, one-way and two-way bending) have been observed in the field [Dizhur et al., 2011].

Walls prone to cantilever failure collapse at far lower excitations compared to those limited to one- or two-way bending: Doherty et al. [2002] showed that the stability of a

cantilever wall is approximately equivalent to that of a simply-supported wall four times more slender. The relatively low cost of installing wall-to-diaphragm anchors is therefore easily justified by the significant improvements in out-of-plane stability provided [Sharif et al., 2007]. Accordingly, the present study focuses on URM walls that have been appropriately anchored to diaphragms, particularly on the least resilient case of one-way bending.

PREVIOUS TESTING

Early experimental work on the topic of out-of-plane URM wall response was restricted to quasi-static testing [Anderson, 1984, Haseltine et al., 1977, Yokel and Dikkers, 1971]. Dynamic testing began with the large-scale programme carried out by ABK Joint Venture [1981], in which 22 wall specimens with different overburden loads and height to thickness (h/t) ratios were tested under dynamic loading. The tests were carried out using displacement-controlled actuators at both the top and bottom of the walls. The issue of diaphragm flexibility was addressed by inputting computer-modelled diaphragm response histories at adjacent levels to the actuators. Cracking was observed near mid-height and at the base of walls, and it was noted that a stable rocking response was possible at relative mid-height displacements significantly in excess of those at crack initiation.

The ABK tests formed the basis for the URM wall assessment procedures in the seismic rehabilitation standard ASCE 41 [ASCE, 2013]. For walls sufficiently anchored to diaphragms, the standard stipulates allowable h/t ratios as a function of the design spectral acceleration, S_a, at a period of 1 s. Several curves are provided based on a wall's location in the building (Figure 1).

Significant additional testing — dynamic, pseudo-dynamic, and static — has been carried out since the ABK project. Shake table tests by Griffith et al. [2004] showed that for rigid-support conditions, the static force-displacement relationship is a reasonable bound of the dynamic hysteretic behaviour, and that wall rocking frequency and damping are both displacement dependent. Meisl et al. [2007] demonstrated that wall rocking behaviour is largely independent of the quality of the collar joints. Tests by Dazio [2008] and Simsir [2004] illustrated the importance of axial load and the manner in which it is applied. Derakhshan et al. [2014] concluded that arching action in walls due to vintage timber diaphragms is negligible, and that the force-displacement characterization obtained in the lab was representative of in-situ conditions. Magenes et al. [2014] subjected three full-

scale stone masonry houses with flexible timber diaphragms to shake table testing. The specimens were retrofitted to various degrees; the observed improvement of the seismic performance in the retrofitted specimens was more attributable to the wall-diaphragm connections than to the stiffening of the diaphragms.

STUDY OBJECTIVES

This study aims to better characterize the out-of-plane seismic response of URM walls, with a focus on the effect of diaphragm flexibility. The study consists of two phases—experimental and numerical. This paper reports on the experimental phase, in which full-scale URM wall specimens were subjected to earthquake ground motions using a shake table, with varying diaphragm stiffness configurations. A companion paper [Penner and Elwood, 2015] presents a numerical study in which the experimental results were used to validate a numerical model, which was in turn used to conduct a large-scale parametric study aimed at improving the assessment of URM walls to out-of-plane excitation. The following sections describe the testing apparatus, the testing protocol, and the shake table test results.

TEST DESCRIPTION

Wall specimens were intended to represent a portion of a top-storey wall in an early 1900s load-bearing URM building in British Columbia. To represent the deterioration of the mortar in existing buildings, a Type O mortar mix (1:2:9 cement:lime:sand by volume) was selected due to its low compressive strength. Brick units were solid clay and measured 64 mm $\times$ 89 mm $\times$ 191 mm. Brick units were placed dry to further minimize the bond strength. While the workmanship in older buildings may be variable, this factor can be difficult to quantify. To achieve reasonable consistency among specimens in this regard, it was therefore decided to employ good construction practices — bricks were precisely placed and collar joints were slushed in all specimens. The age of the walls at testing varied between approximately 2 and 10 months. A detailed description of the specimens and test setup is provided in Penner [2014]; a summary of key features is provided below.

Four 3-wythe walls and one 2-wythe wall were constructed. American bond was used in all walls with a single header course at every sixth course. Specimens are named by diaphragm condition (*[F]lexible*, *[S]tiff*, or *[R]igid* at top and bottom) and the number of

wythes in the wall specimen (e.g. specimen *FR-3* was three wythes thick with a flexible connection at the top of the wall and a rigid connection at the base). A summary of the specimen masses and material properties determined from laboratory testing is provided in Table 1.

The walls were tested on a displacement-controlled single degree of freedom shake table in the Earthquake Engineering Research Facility (EERF) at the University of British Columbia (UBC) using a purpose-built test frame (Figure 2). The test frame imposed a simplified representation of flexible diaphragm boundary conditions on the wall. A stiff steel braced frame, representing the in-plane walls, was constructed on the shake table. The table motion was transferred to the top of this frame with minimal amplification [Penner, 2014]. The inclusion of in-plane wall flexibility was outside the scope of the experimental work. It was instead assumed that the flexibility of the in-plane walls could be considered negligible compared to that of the flexible timber diaphragms.

Top and bottom diaphragms were represented by rolling steel carriages connected to the frame by coil springs. Each coil spring assembly consisted of a pair of springs mounted on a shaft; pre-loading the springs to half-capacity resulted in a system with no 'slop' when transitioning from positive to negative displacement. The carriages were able to roll parallel to the direction of motion of the shake table. Spring stiffnesses were selected to achieve natural periods of vibration in the test setup representative of first-mode in-plane behaviour of typical diaphragm-wall assemblies [Penner, 2014]. The total stiffnesses for each of the top and bottom carriages were 37.0 and 39.4 $\mathrm{kN/m}$ respectively for the flexible springs, and 147 and 142 $\mathrm{kN/m}$ respectively for the stiff springs. Each carriage could also be 'locked out' to simulate a rigid diaphragm condition by connecting the carriage to the braced frame with threaded steel rods. The top and bottom of the wall were connected to the respective carriages. The total carriage masses were estimated to be 663 and 591 kg for the top and bottom, respectively.

The connections between the wall and the carriages constrained the wall's horizontal displacements to match those of the respective carriages, while allowing free vertical displacement and rotation of the wall at both the top and the base. At the base, this was achieved using a stiff rubber spacer, with sliding surfaces lined with low-friction ultra high molecular weight (UHMW) polyethylene. In actual buildings, out-of-plane action on walls would be transmitted partially through the diaphragm and through the wall in the storey be-

low; however, establishing the relative contributions of these two mechanisms was beyond the scope of this study. The experimental conditions represent most of the demand being transmitted through the diaphragm. At the top of the wall, a steel assembly bolted to the wall contained pins protruding past the ends of the wall. The pins travelled within vertical slots in plates mounted to the top carriage. No provisions were made in the test frame for the application of overburden load to the wall beyond that imposed by the steel channel assembly bolted to the top of the wall, which had a mass of approximately 179 kg. The simulations instead concentrated on the worst-case stability conditions found in upper-storey walls with minimal tributary gravity loads.

Instrumentation consisted of displacement transducers and accelerometers, measuring the response of the shake table, test frame, carriages, and the wall specimen. Complete raw and processed data sets as well as project documentation describing the test setup nd instrumentation are archived in the NEES repository [Penner and Elwood, 2014a,b,c,d,e]. All data sets are publicly accessible.

GROUND MOTIONS

Two ground motions were used as input to the shake table, with one motion selected for significant long-period spectral response and the other for a dominant short-period spectral response. The long-period motion selected (CHHC1) was recorded during the 22 February 2011 earthquake in Christchurch, New Zealand at the Christchurch Hospital. The short-period motion selected (NGA0763) was recorded during the 18 October 1989 Loma Prieta earthquake at the Gavilan College in Gilroy, California. Acceleration response spectra as recorded on the shake table are shown in Figure 3 along with design spectra for Seattle, WA, USA and Victoria, BC, Canada, for relative reference. Displacement time histories of the two motions as recorded on the shake table are shown in Figure 4. Scale factors are shown relative to the original motion as recorded during the earthquake, and reference the amplitude of the displacement time history. Wall specimens were full scale, thus no scaling was needed for similitude. The in-plane walls were assumed to be very stiff compared with the diaphragms; the ground motions were therefore not modified for the in-plane response of the building [Penner, 2014].

SHAKE TABLE TESTS

The mortar used in the construction of the test walls (Type O) is of significantly lower strength than that used in modern structural masonry. However, in particular the flexural bond strength of walls found in early 1900s buildings may be weaker still than that of the test walls. It was therefore decided not to rely on the cracking resistance of the test walls in assessing their dynamic stability on the shake table, but rather to assume that the walls would experience cracking at very low levels of excitation.

Accordingly, to ensure that walls would remain stable after crack initiation, allowing further tests to be carried out, cracking was initiated by running the NGA0763 motion with both top and bottom carriages locked out (rigid diaphragm conditions). After cracking was achieved, the carriage connections were adjusted for the desired diaphragm conditions, and subsequent runs were made using the CHHC1 motion at increasing amplitude of input motion until collapse was observed.

VISUAL OBSERVATIONS

Each of the five wall specimens developed a single horizontal crack near mid-height during the tests in which the carriages were locked out. In every case, the crack occurred at the brick-mortar interface, but the crack location varied between the specimens. In wall *RR-3*, the crack was located at a height of 0.74 times the wall height, while in the other four specimens the crack height varied between 0.47 and 0.55 times the wall height (the wall height used to normalize the crack height is taken as the distance from the base of the wall to the centerline of the top pin). Cracks occurred both at header courses and at common courses. In Walls *FF-3*, *FR-3*, and *SS-3*, the crack was located in a single horizontal plane across the entire wall section. In walls *FF-2* and *RR-3*, the crack stepped down by one course. Even after sustained rocking in later runs, all cracks consistently closed up without horizontal offset and with minimal spalling of mortar or brick.

Prior to undergoing significant rigid-body rocking, cracks were visually nearly imperceptible. Walls *FF-2* and *RR-3* underwent the greatest amount of rigid body rocking, and correspondingly also sustained the most spalling damage at the crack. The most severe spalling was limited to roughly the size of a mortar joint; in most walls it was less than this. Every wall underwent rocking about the [wall]-[base beam] interface. No cracking

was observed within the wall near the base. At sufficiently high input motion intensities, each wall specimen eventually underwent rigid-body rocking. Since only a single crack was formed in each wall, the rocking was clearly defined as occurring between two bodies: the lower wall block, from the base beam to the horizontal crack, and the upper wall block, from the crack to the top pin connection. This is illustrated in a video frame of wall *FR-3* just before collapse (Figure 5).

CRACKED RESPONSE SUMMARY

The crack height, system period, and motion scales at collapse and in the run prior to collapse for each specimen are listed in Table 2. The system period is defined independently for the top and bottom of each wall, and should be interpreted as an indicator of the stiffness of each support rather than a true period of response, since the modes of this multi-degree-of-freedom sytem link both the top and bottom responses. In addition, the height of the crack affects the distribution of tributary mass to the top and bottom diaphragms, and once the wall is cracked it no longer exhibits a periodic response [Makris and Konstantinidis, 2003]. For consistency and simplicity, each of these periods is calculated as that of a single degree of freedom linear elastic oscillator using exactly half of the total wall mass plus the mass of the respective carriage system along with the total respective spring stiffness; the period is thus independent of the crack height.

DISPLACEMENT RESPONSE

Once cracked, the wall behaves as two rigid bodies. In the test specimens, the combination of surface friction and potential interlock effect due to a non-planar crack surface effectively prevented any notable sliding at the crack interface. For analysis purposes, the two wall segments were thus assumed to be linked at the crack location. The relative displacements of the wall ends were assumed to be equal to those of the carriages at the base and the top of the wall, which is consistent with the observed performance of the wall-carriage connections during testing.

Displacements of the carriages were measured relative to the table, while displacements of the wall headers were measured relative to the ground (absolute). Displacement nomenclature is illustrated in Figure 6. Rocking displacement, d_{rock}, is defined as the difference between the measured horizontal displacement of the wall at the crack height and the straight-line interpolation between the top and bottom of the wall at the same height.

The normalized rocking displacement, $d_{rock_{norm}}$, is simply the rocking displacement divided by the wall thickness.

Two rocking modes are possible for a wall with a single crack and at least one flexible diaphragm (Figure 7). The main difference between the two cases is the location of the contact point between the upper and lower blocks. In Case 1, the contact point is such that the weight of the upper block acts to stabilize the lower block. In Case 2, the weight of the upper block destabilizes the lower block. While Case 2 rocking can contribute momentum to the lower block that will push it towards collapse, for realistic values of diaphragm stiffness the top block will always flip back into the Case 1 mode before collapse [Penner, 2014].

Displacement time history results of run 10 of wall *FF-2* are shown in Figure 8. This run illustrates sustained rocking behaviour. Three time instants of interest are indicated by the dotted vertical lines. The displacement profiles of the wall at these instants are shown in Figure 9. It can be observed that the rocking displacement becomes zero when the top and bottom rotations are equal, at which point the relative displacement at the crack falls between the top and bottom relative displacements. The largest rocking displacement occurs concurrently with the largest difference in rotations (e.g., at time C, Figure 9c). Note that large rocking displacements can occur while the bottom block is near vertical (e.g., at time A, Figure 9a).

The normalized rocking displacement is plotted for two runs for wall *FF-2* in Figure 10: the highest stable run, and the run causing collapse. This plot illustrates the abrupt change in performance at the out-of-plane wall stability threshold observed in the tests — the response between the two runs is similar in the early portion of the test, until a pulse of sufficiently large magnitude is experienced for the rocking response in the higher run to become unstable, at which point the response histories of the two runs diverge rapidly.

In Figure 11, peak rocking displacement is plotted against the intensity of the ground motion in each post-cracking run. Significant rocking without collapse was observed in four of the five specimens. Wall *FR-3*, with rigid bottom diaphragm condition (e.g. a one-storey building), underwent limited rocking in all runs prior to the collapse run despite large displacements of the top carriage. Of the remaining walls, *FF-3* displayed the least rocking in the run prior to collapse, but presumably this is in large part because the change in intensity was larger between the last two runs for this wall than for the others (20% vs.

5-10%).

The rocking displacement at the crack is compared to the top carriage displacement in Figure 12. The spectral displacement at 1 s is indicated on the y-axis on the right side. The rocking displacements are shown by the heavy solid lines, while the top carriage displacements are shown by the light dashed lines. This plot illustrates that while the carriage (i.e. diaphragm) displacements roughly follow the spectral displacement linearly, the rocking response is fundamentally different.

Makris and Konstantinidis [2003] showed that the rocking response of a simple rectangular block subjected to ground shaking can not be characterized by a single degree of freedom system with a fixed period. Griffith et al. [2004] further determined that the rocking frequency of a cracked wall is displacement dependent. Neither Griffith et al. nor Makris and Konstantinidis had considered the effect of flexible supports in their work.

The 'period' of the rocking response of the walls in the current tests was evaluated by considering each rocking excursion separately. One rocking excursion was defined as the response between adjacent points at which $d_{rock} = 0$. The period of an excursion was defined as two times the duration of the excursion, with one excursion approximating a half-cycle sine pulse. The amplitude of the excursion was recorded as the peak rocking displacement. Amplitudes of less than 5 mm were eliminated due to the limited precision of the measurements from which the rocking displacement was derived. The highest stable run from each wall was considered, with the exception of wall *FR-3*, due the lack of rocking observed. The observed periods are plotted against the corresponding normalized rocking displacements in Figure 13.

The rocking response of all walls follows generally the same trend: the minimum observed period increases as the rocking amplitude increases. For a given rocking amplitude (at moderate values), wall *RR-3* exhibits the overall shortest rocking periods, while the walls with flexible diaphragms exhibit generally longer periods. Wall *RR-3* also produces the most consistently sine-like rocking oscillations; the shape of the rocking excursions of walls with flexible diphragms are more irregular, and one or more direction reversal cycles may be contained within a single rocking excursion. This corresponds with the increased scatter present in Figure 13 for these walls relative to wall *RR-3*.

At smaller rocking amplitudes, the more flexible diaphragms have the capacity to allow

longer rocking periods, but also create greater variability in the rocking period. As the rocking excursions become larger, the effect of diaphragm flexibility becomes less important.

ACCELERATION RESPONSE

A detail of the time history results of run 10 of wall *SS-3* are shown in Figure 14. This run illustrates a large rocking excursion and the associated impact when the crack closes up. Three time instants of interest are indicated by the vertical dashed lines. Figures 14a and 14b show the relative displacements and the rocking displacement, respectively, while Figure 14c shows the accelerations of the top and bottom carriages and the calculated mean acceleration at the crack.

The acceleration time history during rocking is characterized by periods of relatively smoothly varying accelerations during rocking excursions followed by periods of rapid variation following the impacts caused by the crack closing up. Peak accelerations at the crack and at the carriages occur at impact times.

At the peak of the large rocking excursion (time A, Figure 14), relative velocities of the carriages and of the crack are small, and the crack acceleration is in the opposite direction of the carriage accelerations—they are accelerating towards closing up the crack. The accelerations slowly converge as the crack closes up, until roughly 0.015 s before the impact point (time B), at which point the acceleration profile is fairly uniform. The crack is now moving in the negative direction with considerable velocity, while the carriages are moving slightly in the positive direction. As the crack now closes, the wall at crack height quickly picks up positive acceleration (slowing its negative travel) while the carriages pick up negative acceleration. Peak acceleration is reached roughly 0.015 s after the crack has closed (time C). The rocking response of the wall has therefore dragged the carriages 'along for the ride', demonstrating that significant two-way interaction can occur between walls and diaphragms under the right conditions.

In this case, the carriages were lighter than the wall, facilitating this two-way interaction. If the carriages had been much heavier than the wall, the carriage motions would have approached that predicted for SDOF oscillators, and the wall would have been 'along for the ride' instead. It is likely that in this case, there would have been a larger rocking excursion following the main excursion, as the cracked wall would snap through between

the carriages while they would carry on moving in their original (opposite) direction. It is expected that this characteristic would reduce the overall stability of the system. This hypothesis is supported by analysis of the high mass diaphragm condition [Penner, 2014].

The peak accelerations calculated at the crack height are shown in Figure 15 for each post-cracking run. Peak crack accelerations increased mainly monotonically for walls *FF-3*, *FF-2*, and *SS-3*, and remained fairly constant for walls *FR-3* and *RR-3*. The lack of large increases for *FR-3* are again likely due to the lack of large rocking impacts. In contrast, wall *RR-3* was subject to large rocking impacts without significant increases in crack accelerations. The fixed diaphragm conditions appear to dampen the acceleration peaks by preventing the 'flicking' effect at snap-through that is allowed by the flexible diaphragms. With a fixed diaphragm, a wall segment pivots about the diaphragm connection, while with a flexible diaphragm, the effective pivot is located within the wall segment, allowing snap-through to occur more violently by accelerating both ends of the wall segment in opposite directions.

FORCE RESPONSE

The acceleration profile of a cracked wall is the sum of several components, as illustrated in Figure 16. The total force is the integration of this profile along with the mass density over the height; as such it is a high-level quantity, and consequently details about the response can be hidden within it. Two significantly different acceleration profiles can produce the same total force. For example, a uniform profile equal to zero everywhere on the wall and a profile with large accelerations at the crack and at each carriage, where the crack acceleration has the opposite sign as that at the carriages, can both produce a total force that is equal to zero even though the wall response is very different at those two times.

Peak total force demands for each post-cracking run, as calculated from measured wall accelerations, are plotted in Figure 17. Forces are presented as normalized to the wall weight in units of 'g', thus indicating the equivalent inertial force. In general, trends for each wall are fairly linear, with some 'softening' possible towards the collapse run (i.e. the point for the collapse run exhibits a lower maximum force than a linear extrapolation from the other runs would suggest). Wall *FF-3* showed the greatest deviation from linearity in the collapse run, while in other walls the effect was less notable. The specimens with the flexible springs (*FF-3*, *FR-3*, and *FF-2*) showed a generally lower rate of change of force

with respect to motion intensity than the stiff and rigid specimens, with *FR-3* showing the lowest rate by a significant margin.

Individual connection forces were calculated based on carriage displacement and spring rates, with a correction for carriage inertial force. This was only possible for non-rigid diaphragm conditions—when a carriage is locked into the rigid mode, the stiffness is too high and the displacements are too low to reliably measure the spring force. For specimens with non-rigid connections at both top and bottom, total force demands were calculated as the sum of the connection demands. These results generally agreed closely with total force demands calculated from wall inertia [Penner, 2014].

Peak demands calculated using both methods (as applicable) are listed for the highest stable run and for the collapse run in Table 3. Here, total forces are normalized to the total wall weight, while individual connection forces are normalized to 50% of the wall weight—representative of the way in which tributary wall weights would be assigned in the assessment of a real building. Motion scales for the runs noted are listed in Table 2. Since calculated connection forces are based on displacement measurements, they tend to smooth off short duration force peaks. Total wall forces based on acceleration measurements capture such force peaks more accurately, resulting in some discrepancy between peak forces calculated by the two methods in runs with large rocking impacts. Discrepancies were only significant in some of the runs causing collapse; in stable runs, where connection demands are of concern, the two methods produced very similar results.

The maximum recorded total normalized force for a cracked wall calculated by either method, in any run, is 0.61 g. This includes forces caused by impact when cracks close up, and includes collapse runs (up to a rocking displacement of just over one wall thickness).

Peak force demands were compared with those predicted using the spectral acceleration of the shake table motion at the diaphragm period. Damping values obtained from calibration of a numerical model were used [Penner and Elwood, 2015]. Periods, damping ratios, and S_a values at 100% scale are shown in Table 4. Note that these damping ratios are strictly intended to represent the testing apparatus; a consensus on appropriate damping ratios for timber diaphragms in real buildings has yet to be reached. Wilson [2012] suggested a value of 5 % may be appropriate, while in-situ testing by Giongo et al. [2015] indicated values of 10 to 30 % may be more realistic. Using the experimental parameters, the force demands listed in Table 3 are compared to the corresponding scaled S_a values in Table 5.

The results indicate that the spectral acceleration is in general a reasonable approximate predictor of demands.

However, forces significantly higher than those predicted by this method were observed, particularly for the bottom connection demand. In stable runs, connection force demands up to 1.5 times higher than predicted were observed. These high demands appear to be caused by the impacts induced when the crack closes up after large rocking excursions. Although somewhat higher force amplification factors were observed in runs causing collapse, peak demands in stable runs are of primary interest for the design of connections. These observations emphasize that rocking cannot be relied upon to reduce anchorage demands, but rather that the impacts caused by rocking can potentially amplify anchorage demands. In addition, the capability of anchors to accommodate the rotation of the wall during rocking without deterioration should be considered during design; the experimental testing did not account for anchor deformation limitations.

FORCE DEMANDS AT CRACKING

Cracking was initiated in each wall by subjecting it to the NGA0763 motion with both carriages locked into the rigid mode. Total wall forces were calculated in these runs based on wall inertia. The time of crack initiation was calculated based on the shape of the acceleration profile—a distinct change from a curved to bilinear shape was observed in each wall [Penner, 2014]. In the cracking runs, the local force peak at the time of crack initiation is not necessarily the maximum force attained in that run. This suggests that cracks are formed progressively—some damage is caused during the large initial force peaks, but not enough to propagate the crack through the entire wall thickness. Subsequent force peaks, though smaller, cause further damage until eventually the crack has propagated through the wall.

The total wall forces in the cracking run are compared with those measured in the two highest cracked runs for each wall in Table 6. Maximum forces for each wall are shown in bold. For cracking runs, both the peak force at the time of crack initiation and the maximum force recorded during the entire run (which in some cases occurred well before crack intiation) are listed. Maximum forces attained in the highest stable rocking runs were lower in each case than those attained during the cracking runs. During collapse runs, force levels in walls *FF-3* and *SS-3* exceeded those attained during the respective cracking runs.

In all cases, maximum wall forces recorded were between 0.5 and 0.6 g.

The wall forces in the cracking runs in Table 6 are equal to the sum of the top and bottom connection demands, which are representative of the demands on wall-to-diaphragm anchors. By assuming the wall to be pin supported at the connections, the total force demand was calculated to be allocated to the top and bottom connections as between 50%/50% and 60% top/40% bottom. Note that these allocations are based on the observed values from this particular test apparatus only, and they do not necessarily reflect conditions that may be encountered in real buildings.

Flexural cracking, as observed in the test specimens, is initiated when the tensile bond strength of the wall is exceeded. Axial stresses across the height and thickness of the wall were calculated through simple statics at each measured time step for the cracking runs [Penner, 2014]. The location of the peak tensile stress varies significantly, and is plotted as a function of the stress for wall *FF-3* in Figure 18, for all measurement points occurring prior to cracking.

The height of the point of peak tensile stress consistently decreases as the stress increases. At the largest stresses (those that would initiate cracking), the peak stress occurs at approximately 55% of the wall height. This trend, including the location at high stresses, was consistent among all specimens. This indicates that the variability in crack height among specimens (Table 2) can likely be attributed to the details of each wall's construction—the strength of each joint in the wall will not be the same due to construction variability and errors—rather than to a significant difference in demands imposed upon the wall.

Peak tensile stresses at crack initiation showed good agreement with flexural tensile strength values obtained from bond wrench testing [Penner, 2014]. It is concluded that the maximum force demands imposed on wall-diaphragm connections by an uncracked wall can be assumed to be governed by the wall's design flexural tensile strength. Connection capacities should be checked against the maximum demands imposed by both uncracked and cracked walls.

CONCLUSIONS

A dynamic testing programme was developed and conducted at the University of British Columbia's Earthquake Engineering Research Facility with the objective of generating a data set to be used for validation of a numerical model. Five full-scale unreinforced solid clay brick wall specimens spanning one storey were subjected to earthquake ground motions on a shake table. The top and bottom of the walls were connected to the shake table through coil springs, simulating the flexibility of the diaphragms. The apparatus allowed the wall supports to undergo large absolute displacements, as well as out-of-phase top and bottom displacements, consistent with the expected performance of URM buildings with timber diaphragms. Variables examined included diaphragm stiffness and wall height.

Walls were cracked by applying a ground motion under rigid diaphragm conditions, then tested to failure with flexible diaphragm conditions by incrementally increasing the intensity of the applied ground motion. All walls sustained horizontal cracks at an intermediate height, with four out of five walls cracking between 0.47 and 0.55 times the wall height, and one wall cracking at 0.74 times the wall height. It was determined that the maximum force demands imposed on wall-diaphragm connections by an uncracked wall can be assumed to be governed by the wall's design flexural tensile strength.

The ground motion intensity at collapse varied widely among the walls with different boundary conditions. The lowest level causing collapse was 65% of the as-recorded amplitude, while the highest was 120%. In general, walls connected to more flexible diaphragms sustained higher motion intensities before collapse; however, this observation is specific to the single ground motion used in the testing programme and should not be interpreted as representative of a general trend for all ground motions. The effect of ground motion variability is examined in depth in the companion paper [Penner and Elwood, 2015].

Extensive stable rocking was observed in some specimens, while in others the amount of rocking was limited. The specimen with rigid diaphragm conditions exhibited the most rocking cycles in the run prior to collapse. The specimen with a flexible top diaphragm and rigid bottom diaphragm exhibited effectively no rocking until collapse, yet withstood the highest intensity of ground motion.

Force demands on wall-diaphragm connections at the top and base of walls in stable runs were observed to be up to 1.5 times those predicted from the spectral acceleration

of the input ground motion at the period of the diaphragm-wall systems. Demands on the bottom connection were consistently larger than on the top connection, which may be due in part to the base moment exerted by the self-weight of the wall with respect to the corner contact point. These observations emphasize that rocking cannot be relied upon to reduce anchorage demands, but rather that the impacts caused by rocking can amplify anchorage demands. Further study is required to determine if this amplification is consistent for other ground motions and wall conditions. Anchor capacities should be checked against the maximum demands imposed by both uncracked and cracked walls, and the capability of anchors to accommodate the rotation of the wall during rocking without deterioration should be considered.

In the second phase of this study, the experimental results described herein were used to validate a numerical model, which in turn was used to conduct a large-scale parametric study on out-of-plane wall stability. The scope of the numerical study includes the effects of ground motion variability and numerous parameters that could not be examined as part the experimental study. The numerical study is described in a companion paper [Penner and Elwood, 2015].

REFERENCES

ABK Joint Venture (1981). "Methodology for mitigation of seismic hazards in existing unreinforced masonry buildings: Wall testing, out-of-plane." *ABK Topical Report 04*, National Science Foundation, El Segundo, California.

Anderson, C. (1984). "Arching action in transverse laterally loaded masonry wall panels." *The Structural Engineer*, 62B(1), 12–23.

ASCE (2013). "Seismic evaluation and retrofit of existing buildings." *ASCE 41-13*, Reston, VA, USA.

ASTM (2010). "Standard test method for measurement of masonry flexural bond strength." *ASTM C1072 - 10*, West Conshohocken, PA, USA.

ASTM (2011). "Standard test method for compressive strength of masonry prisms." *ASTM C1314 - 11a*, West Conshohocken, PA, USA.

Bruneau, M. and Lamontagne, M. (1994). "Damage from 20th century earthquakes in eastern Canada and seismic vulnerability of unreinforced masonry buildings." *Canadian Journal of Civil Engineering*, 21(4), 643–662.

CSA (2009). "Mortar and grount for unit masonry." *CAN/CSA A179-04 (R2009)*, Mississauga, ON, Canada.

Dazio, A. (2008). "The effect of the boundary conditions on the out-of-plane behavior of unreinforced masonry walls." *14th World Conference on Earthquake Engineering*.

Derakhshan, H., Dizhur, D., Griffith, M. C., and Ingham, J. M. (2014). "In situ out-of-plane testing of as-built and retrofitted unreinforced masonry walls." *Journal of Structural Engineering*, 140(6), 04014022.

Dizhur, D., Ingham, J., Moon, L., Griffith, M., Schultz, A., Senaldi, I., Magenes, G., Dickie, J., Lissel, S., Centeno, J., et al. (2011). "Performance of masonry buildings and churches in the 22 February 2011 Christchurch earthquake." *Bulletin of the New Zealand Society for Earthquake Engineering*, 44(4), 279–296.

Doherty, K., Griffith, M. C., Lam, N., and Wilson, J. (2002). "Displacement-based seismic analysis for out-of-plane bending of unreinforced masonry walls." *Earthquake engineering & structural dynamics*, 31(4), 833–850.

519 Giongo, I., Dizhur, D., Tomasi, R., and Ingham, J. M. (2015). "Field testing of flexible
520 timber diaphragms in an existing vintage URM building." *Journal of Structural Engi-*
521 *neering*, 141(1), D4014009.

522 Griffith, M. C., Lam, N. T., Wilson, J. L., and Doherty, K. (2004). "Experimental investiga-
523 tion of unreinforced brick masonry walls in flexure." *Journal of Structural Engineering*,
524 130(3), 423–432.

525 Haseltine, B., West, H., and Tutt, J. (1977). "The resistance of brickwork to lateral loading.
526 Part 2. Design of walls to resist lateral loads." *The Structural Engineer*, 55(10), 422–30.

527 Magenes, G., Penna, A., Senaldi, I. E., Rota, M., and Galasco, A. (2014). "Shaking ta-
528 ble test of a strengthened full-scale stone masonry building with flexible diaphragms."
529 *International Journal of Architectural Heritage*, 8(3), 349–375.

530 Makris, N. and Konstantinidis, D. (2003). "The rocking spectrum and the limitations of
531 practical design methodologies." *Earthquake engineering & structural dynamics*, 32(2),
532 265–289.

533 Meisl, C. (2006). "Out-of-plane seismic performance of unreinforced clay brick masonry
534 walls." M.S. thesis, University of British Columbia, Canada.

535 Meisl, C., Elwood, K., and Ventura, C. (2007). "Shake table tests on the out-of-plane re-
536 sponse of unreinforced masonry walls." *Canadian Journal of Civil Engineering*, 34(11),
537 1381–1392.

538 Penner, O. (2014). "Out-of-plane dynamic stability of unreinforced masonry walls con-
539 nected to flexible diaphragms." Ph.D. thesis, University of British Columbia, Canada.

540 Penner, O. and Elwood, K. (2014a). "Shake table testing of out-of-plane URM wall —
541 Wall A (flexible/flexible, 3-wythe)." *Network for Earthquake Engineering Simulation*
542 *(NEES)(distributor)*, Dataset(DOI: 10.4231/D3WD3Q26Z).

543 Penner, O. and Elwood, K. (2014b). "Shake table testing of out-of-plane URM wall
544 — Wall B (flexible/rigid, 3-wythe)." *Network for Earthquake Engineering Simulation*
545 *(NEES)(distributor)*, Dataset(DOI: 10.4231/D3RN30826).

Penner, O. and Elwood, K. (2014c). "Shake table testing of out-of-plane URM wall — Wall C (flexible/flexible, 2-wythe)." *Network for Earthquake Engineering Simulation (NEES)(distributor)*, Dataset(DOI: 10.4231/D3MW28F8F).

Penner, O. and Elwood, K. (2014d). "Shake table testing of out-of-plane URM wall — Wall D (rigid/rigid, 3-wythe)." *Network for Earthquake Engineering Simulation (NEES)(distributor)*, Dataset(DOI: 10.4231/D3H41JN53).

Penner, O. and Elwood, K. (2014e). "Shake table testing of out-of-plane URM wall — Wall E (stiff/stiff, 3-wythe)." *Network for Earthquake Engineering Simulation (NEES)(distributor)*, Dataset(DOI: 10.4231/D3CF9J73N).

Penner, O. and Elwood, K. (2015). "Out-of-plane dynamic stability of unreinforced masonry walls: parametric study and assessment guidelines." *Earthquake Spectra*, xx(xx), xx–xx.

Russell, A., Elwood, K., and Ingham, J. (2013). "Lateral force-displacement response of unreinforced masonry walls with flanges." *Journal of Structural Engineering*, 140(4), 4013087.

Sharif, I., Meisl, C., and Elwood, K. (2007). "Assessment of ASCE 41 height-to-thickness ratio limits for urm walls." *Earthquake Spectra*, 23(4), 893–908.

Simsir, C. (2004). "Influence of diaphragm flexibility on the out-of-plane dynamic response of unreinforced masonry walls." Ph.D. thesis, University of Illinois at Urbana-Champaign, USA.

Wilson, A. (2012). "Seismic assessment of timber floor diaphragms in unreinforced masonry buildings." Ph.D. thesis, University of Auckland, New Zealand.

Yokel, F. Y. and Dikkers, R. D. (1971). "Strength of load bearing masonry walls." *Journal of the Structural Division*, 97(5), 1593–1609.

TABLE 1: Specimen properties

Walls	Mortar compression[a] f'_j (MPa)	c_v	Masonry compression[b] f'_m (MPa)	c_v	Flexural bond[c] f'_{fb} (MPa)	c_v	Wall mass (kg)	Wall dimensions $L \times W \times H$ (mm)
FF-3							3627	1509×291×3947
FR-3	4.0	0.23	33	0.20	0.38	0.42	3614	1500×291×3984
FF-2							1739	1504×191×2790
SS-3	4.2	0.35	46	0.13	0.55	0.31	3833	1518×300×3985
RR-3							3768	1513×296×3973

[a] CAN/CSA A179-04 (R2009) [CSA, 2009]
[b] ASTM C1314 - 11a [ASTM, 2011]
[c] ASTM C1072 - 10 [ASTM, 2010]

TABLE 2: Results summary

Wall	Normalized crack height	Period (s)		Motion scale	
		Top	Bottom	Highest stable run	Collapse run
FF-3	0.47	1.63	1.55	80%	100%
FR-3	0.55	1.62	0	110%	120%
FF-2	0.49	1.28	1.21	110%	120%
SS-3	0.51	0.83	0.83	75%	80%
RR-3	0.74	0	0	60%	65%

TABLE 3: Peak normalized force demands (g)

	Highest stable run					Collapse run				
		Wall	Connection				Wall	Connection		
Wall	Run	Total	Total	Top	Bot.	Run	Total	Total	Top	Bot.
FF-3	12	0.26	0.28	0.23	0.38	13	0.58	0.47	0.41	0.53
FR-3	9	0.31	—	0.31	—	10	0.33	—	0.33	—
FF-2	10	0.35	0.36	0.25	0.49	11	0.39	0.38	0.35	0.55
SS-3	12	0.44	0.42	0.34	0.52	13	0.58	0.50	0.39	0.61
RR-3	5	0.30	—	—	—	7	0.33	—	—	—
Maximum:		0.44	0.42	0.34	0.52		0.58	0.50	0.41	0.61

Total wall forces are normalized to total wall weight
Top and bottom connection forces are each normalized to one-half of the wall weight
For wall *RR-3*, Run 6 was run at a lower amplitude than than the preceding Run 5 to obtain an additional data point prior to collapse

TABLE 4: Period, damping, and full-scale S_a values

Wall	T_s (s)	ζ	$S_a(T_s)_{100\%}$ (g)
FF-3	1.59	0.08	0.35
FR-3	1.59	0.08	0.35
FF-2	1.24	0.12	0.31
SS-3	0.83	0.08	0.49
RR-3	0	0.08	0.50[a]

[a] PGA

TABLE 5: Ratio of peak normalized force demands to $S_a(T_s)$

	Highest stable run					Collapse run				
		Wall	Connection				Wall	Connection		
Wall	Run	Total	Total	Top	Bot.	Run	Total	Total	Top	Bot.
FF-3	12	0.94	1.03	0.84	1.39	13	1.69	1.36	1.17	1.54
FR-3	9	0.81	—	0.82	—	10	0.78	—	0.80	—
FF-2	10	1.04	1.08	0.75	1.46	11	1.05	1.04	0.94	1.50
SS-3	12	1.20	1.15	0.93	1.42	13	1.49	1.28	1.00	1.56
RR-3	5	1.00	—	—	—	7	1.01	—	—	—
Maximum:		1.20	1.15	0.93	1.46		1.69	1.36	1.17	1.56

Total wall forces are normalized to total wall weight
Top and bottom connection forces are each normalized to one-half of the wall weight

TABLE 6: Peak normalized forces in cracking run and cracked runs (g)

	Cracking run		Cracked runs	
Wall	Initiation	Entire run	Highest stable	Collapse
FF-3	0.39	0.40	0.26	**0.58**
FR-3	0.36	**0.52**	0.31	0.33
FF-2	**0.58**	**0.58**	0.35	0.39
SS-3	0.30	0.49	0.44	**0.58**
RR-3	0.49	**0.50**	0.30	0.33

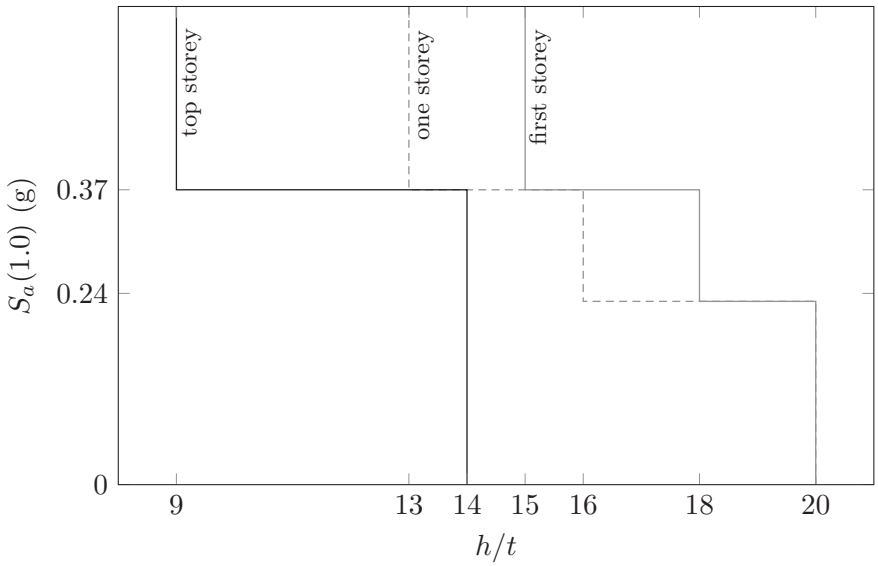

FIG. 1: ASCE 41 h/t limits

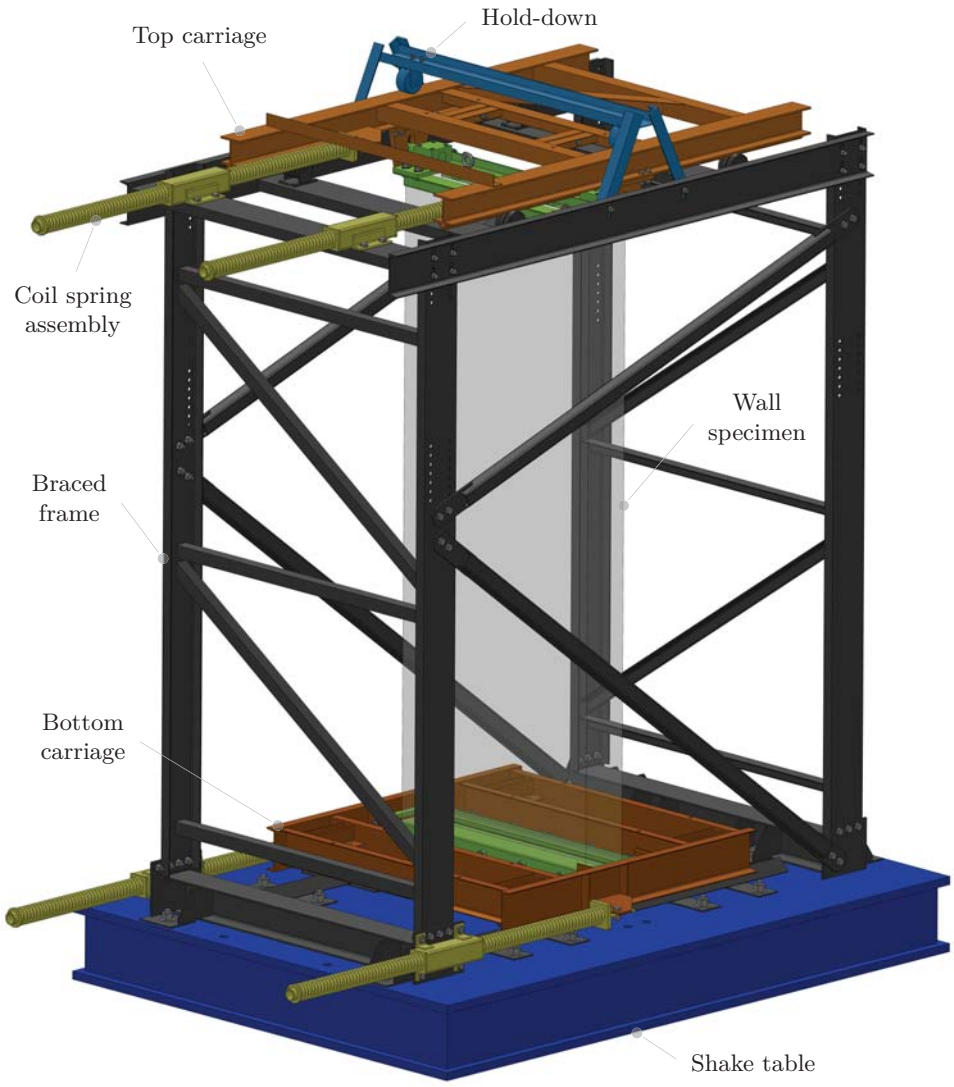

FIG. 2: Model depiction of test apparatus

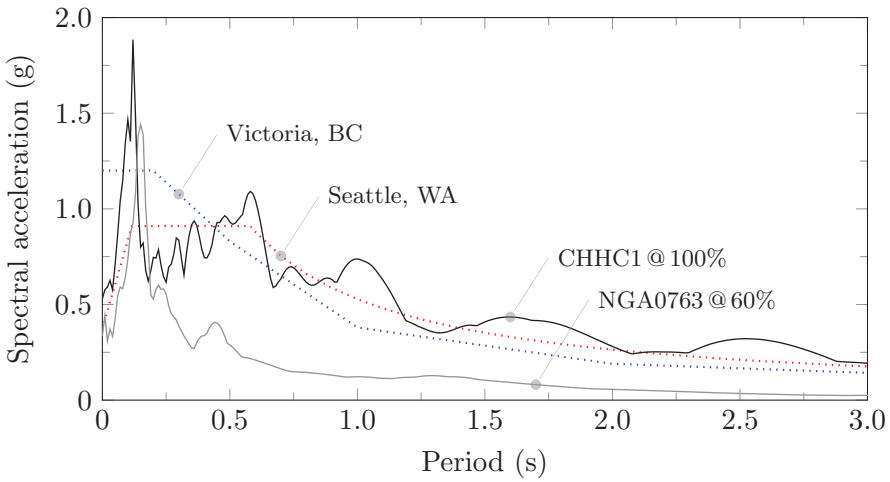

FIG. 3: Response spectra of recorded table motions (5% damped elastic)

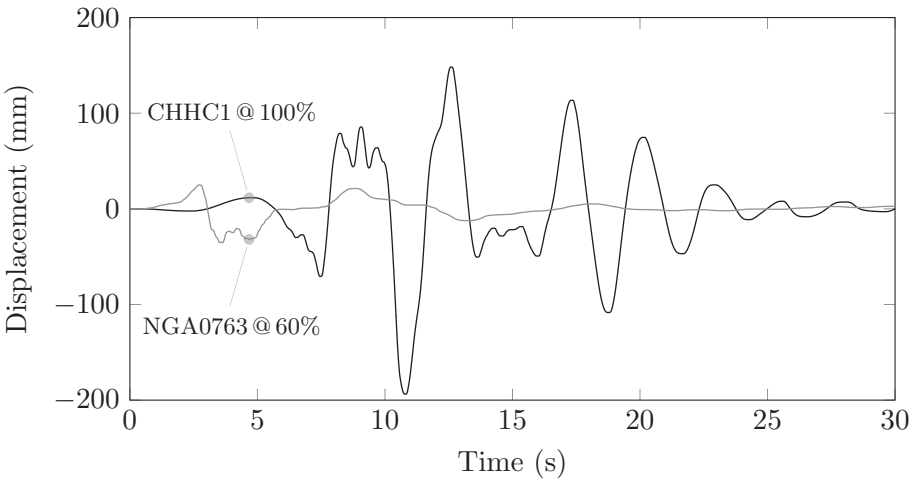

FIG. 4: Table displacement time history

FIG. 5: Wall rocking before collapse

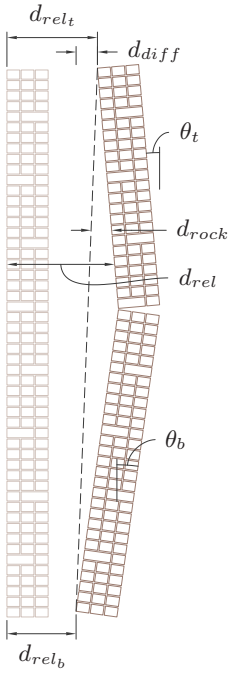

FIG. 6: Displacement nomenclature

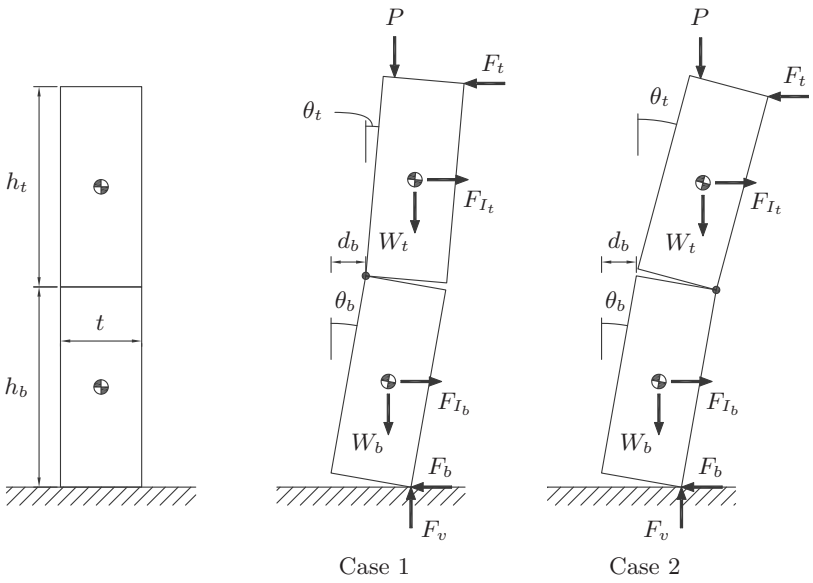

FIG. 7: Rocking mode shapes

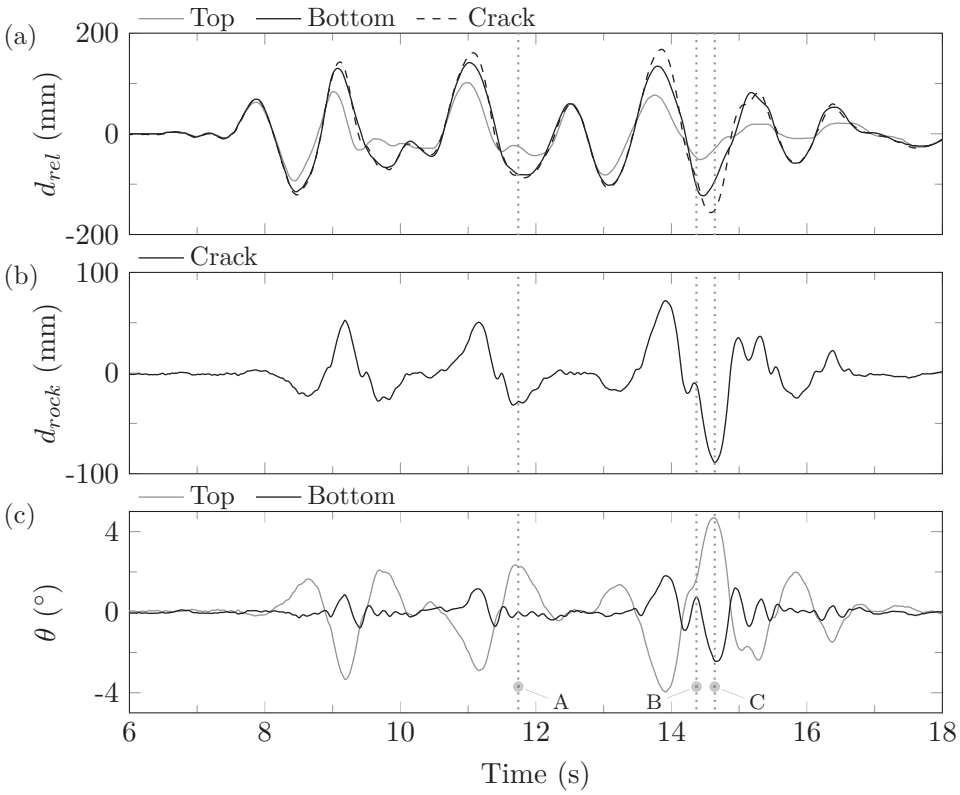

FIG. 8: Displacement time histories, wall *FF-2*, run 10

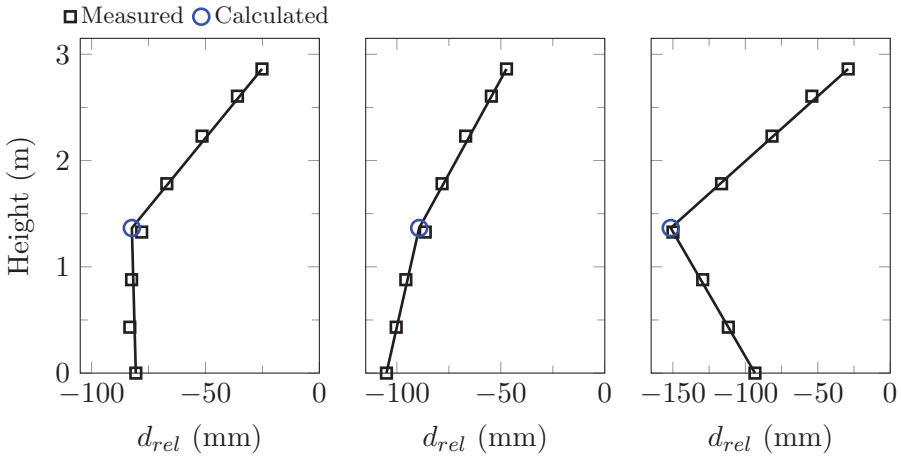

(a) Time A (b) Time B (c) Time C

FIG. 9: Displacement profiles, wall *FF-2*, run 10

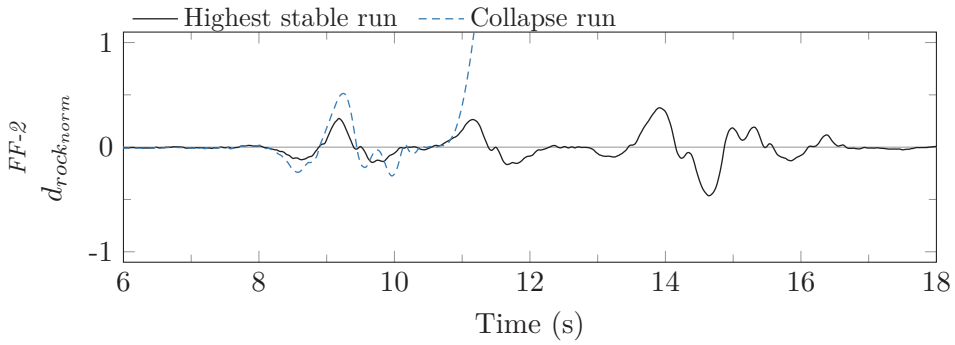

FIG. 10: Rocking time histories, highest stable and collapse runs

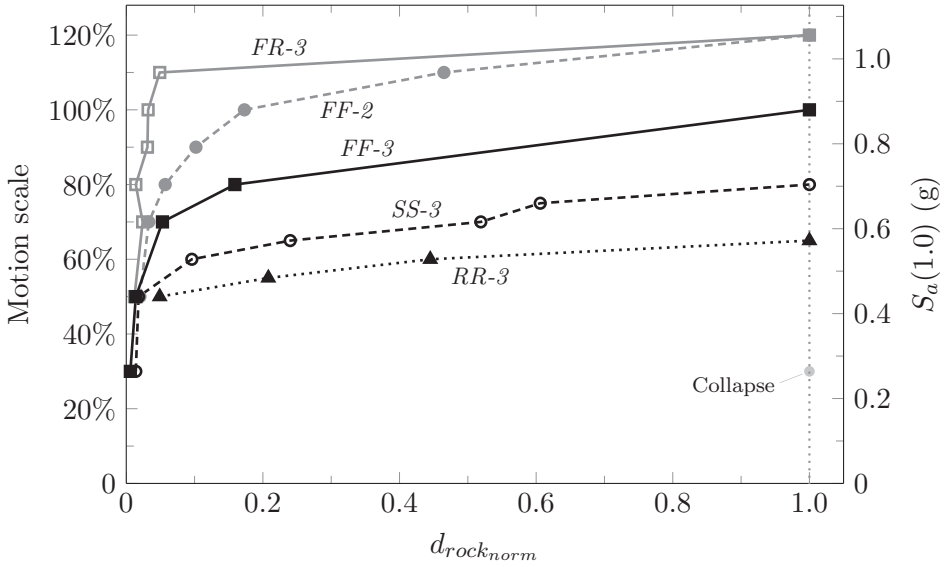

FIG. 11: Peak rocking displacements

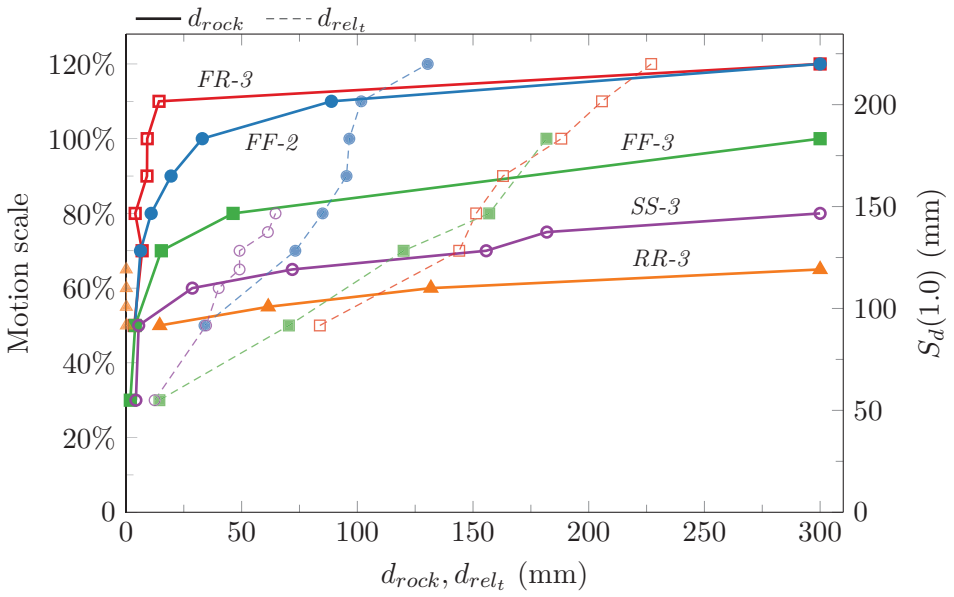

FIG. 12: Peak top carriage and rocking displacements vs. S_d

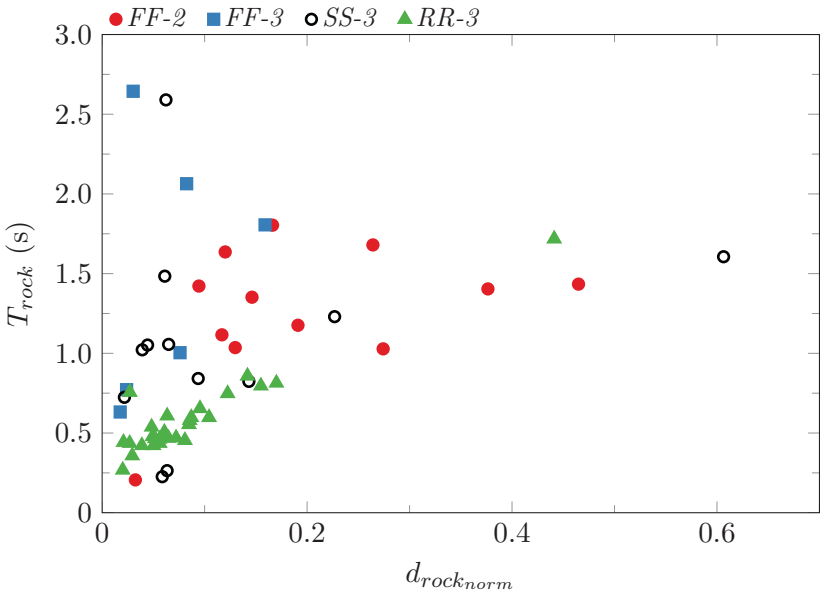

FIG. 13: Rocking period

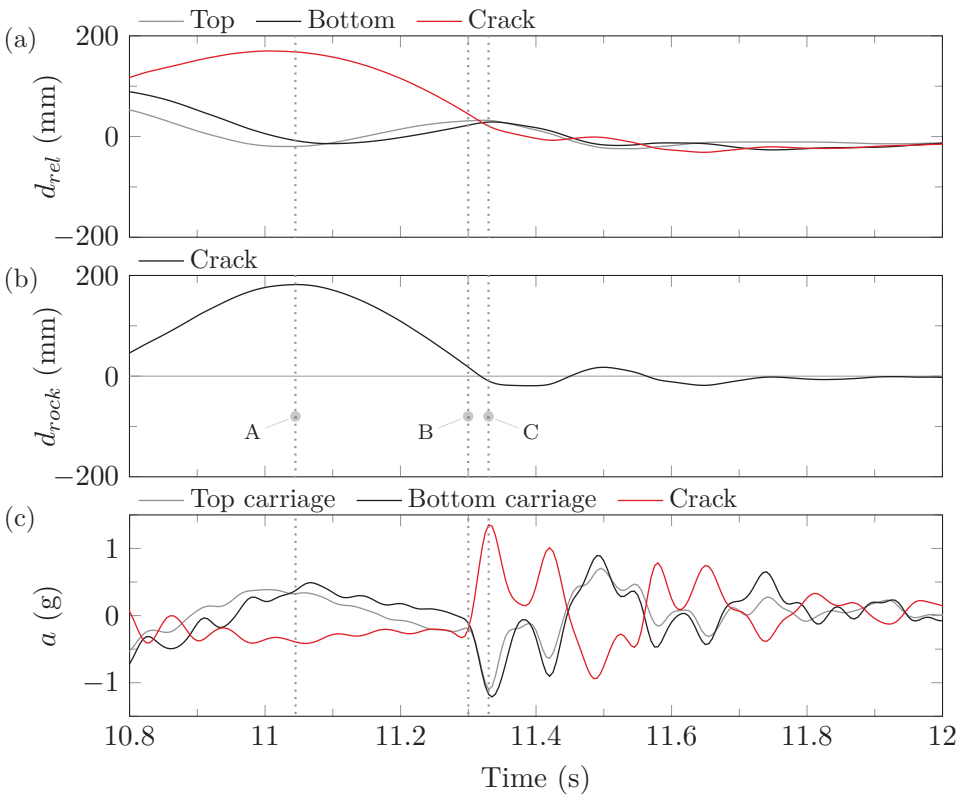

FIG. 14: Close-up of acceleration and displacement time histories, wall *SS-3*, run 12

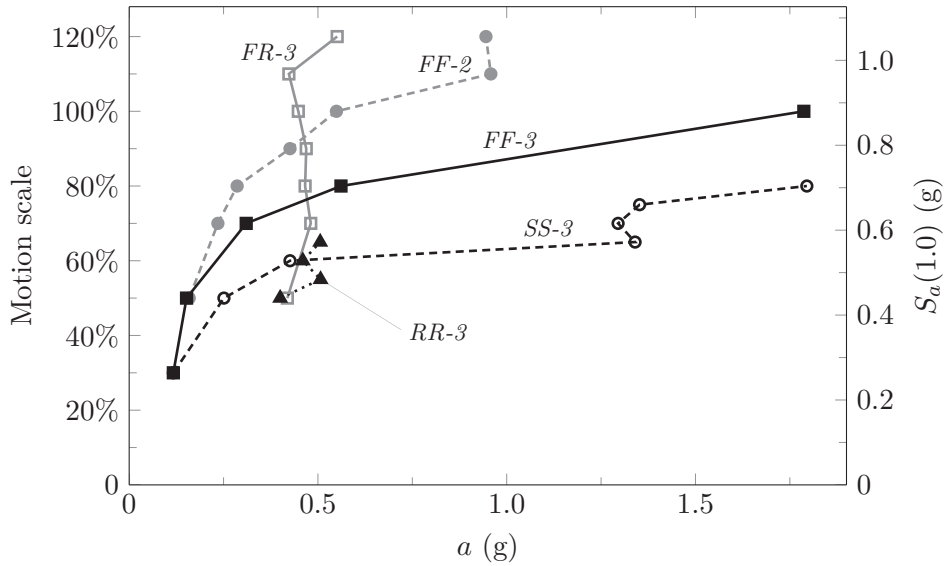

FIG. 15: Peak wall accelerations at crack

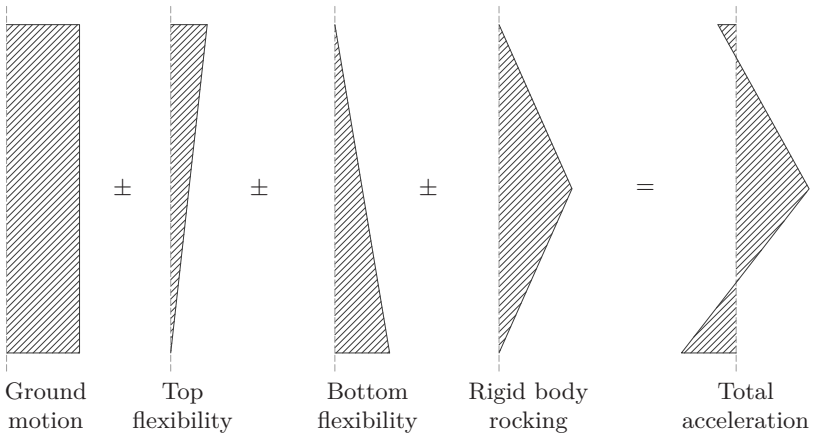

FIG. 16: Components of acceleration profile (adapted from [Meisl, 2006])

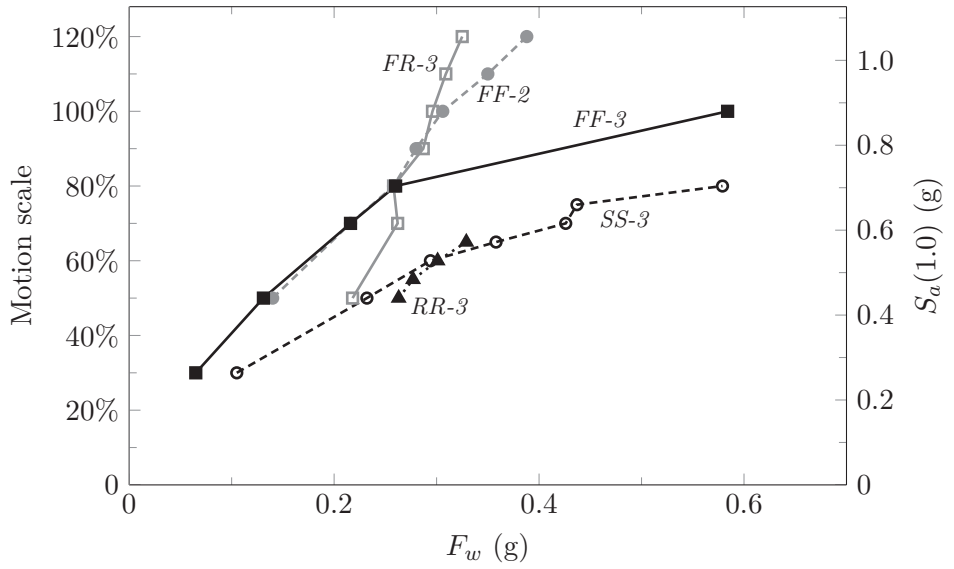

FIG. 17: Peak normalized force demands on cracked wall

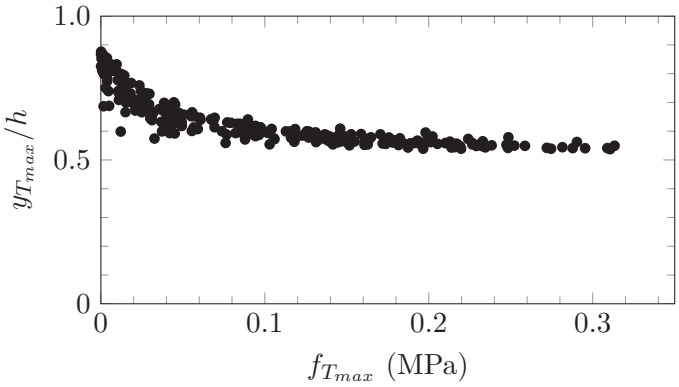

FIG. 18: Location of peak tensile stress, wall *FF-3*, cracking run